Small band gap D–π–A–π–D benzothiadiazole derivatives with low-lying HOMO levels as potential donors for applications in organic photovoltaics: A combined experimental and theoreti…

ARTICLE *in* RSC ADVANCES · AUGUST 2014

Impact Factor: 3.84 · DOI: 10.1039/C4RA02700K

RSC Advances

PAPER

View Article Online
View Journal | View Issue

Cite this: *RSC Adv.*, 2014, **4**, 35318

Small band gap D-π-A-π-D benzothiadiazole derivatives with low-lying HOMO levels as potential donors for applications in organic photovoltaics: a combined experimental and theoretical investigation†

Mahalingavelar Paramasivam,[ab] Akhil Gupta,[c] Aaron M. Raynor,[c] Sheshanth V. Bhosale,*[c] K. Bhanuprakash*[ad] and V. Jayathirtha Rao*[bd]

Received 27th March 2014
Accepted 21st July 2014

DOI: 10.1039/c4ra02700k

www.rsc.org/advances

In an attempt to develop small organic molecules with potential applications as donors in organic photovoltaic (OPV) devices, we have synthesized and characterized four novel benzothiadiazole (A) core structured D-π-A-π-D dyes featuring carbazole and benzocarbazole as donors (D) and fluorene and thiophene as spacers (π). The effects of the π-spacer units and variations in donor strength on the photophysical, electrochemical and thermal properties of the molecules have been investigated in detail. The replacement of fluorene by thiophene as a π-spacer promotes planarity, resulting in a larger bathochromic absorption shift, enhanced emission profiles and an enhanced intramolecular charge transfer (ICT) transition. The introduction of the benzocarbazole unit creates a low-lying HOMO level, as inferred from cyclic voltammetry studies. All the dyes exhibit remarkable thermal robustness. Theoretical calculations have been carried out to understand the structure–property relationships of the synthesized materials. The results obtained from the characterization methods reveal that the dyes with thiophene π-spacers show better optoelectronic properties compared to their fluorene counterparts. Solution-processable bulk-heterojunction devices with a structure of ITO/PEDOT:PSS (38 nm)/active layer/Ca (20 nm)/Al (100 nm) were fabricated using the materials investigated in this study as donors and (6,6)-phenyl C_{61}-butyric acid methyl ester ($PC_{61}BM$) as an acceptor. A power conversion efficiency of 1.62% for the molecule with thiophene as a spacer and carbazole as donor/$PC_{61}BM$ was achieved for the preliminary photovoltaic devices under simulated AM 1.5 illumination (100 mW cm^{-2}).

Introduction

The quest to produce clean and renewable energy by developing organic π-conjugated molecules for organic photovoltaic (OPV) applications has attracted considerable attention from researchers over the last few decades.[1] Early on, organic solar cells were prepared using polymers as light harvesting electron donors owing to their high optical density, optimized film morphology and other superior properties.[2] Despite having these unique features, polymers face the problems of polydispersity, variation between batches and complex purification procedures, thus paving the way for small organic molecules as emergent alternatives.[3,4] Initially, small molecules as electron donors lagged behind the polymers due to their inferior photovoltaic performance, even though small molecules have several advantages including facile synthesis, well-defined molecular structures, amenability for large scale production and so on. Later, the efficiency of small molecule organic solar cells began to gradually evolve, reaching 8.2% efficiency through scrutinized molecular design.[5] Recently, Heliatek, a German company, reported tandem solar cells featuring small molecules with the unprecedented cell efficiency of 12% for a standard size of 1.1 cm^2.[6] In view of this trend, the day may not be far off when small-molecule organic solar cells will outperform their polymer counterparts.

To improve the photovoltaic performance of small molecules, many factors such as light absorption, charge carrier transport, carrier injection, charge separation, *etc.* should be considered.[7] An elegant strategy is to design the backbone structures of these small molecules by the combination of

[a]*Inorganic and Physical Chemistry Division, CSIR-Indian Institute of Chemical Technology, Hyderabad, 500007, India. E-mail: bhanu2505@yahoo.co.in*

[b]*Crop Protection Chemicals Division, CSIR-Indian Institute of Chemical Technology, Hyderabad, 500007 India. E-mail: jrao@iict.res.in*

[c]*School of Applied Sciences, RMIT University, GPO Box 2476V, Melbourne, Victoria 3001, Australia. E-mail: sheshanath.bhosale@rmit.edu.au*

[d]*CSIR-Network of Institutes for Solar Energy, New Delhi, India*

† Electronic supplementary information (ESI) available. See DOI: 10.1039/c4ra02700k

various π-building blocks, with the following points in mind: (1) to improve the photocurrent (J_{sc}), the molecule must have a small HOMO–LUMO gap without sacrificing V_{oc}; (2) to match the frontier energy levels, which are mostly dependent on the chemical structures of individual π-building blocks, with the electron acceptors such as [6, 6]-phenyl- C_{61}-butyric acid methyl ester ($PC_{61}BM$), and perylenediimides (PDI) so as to facilitate the rate of electron injection efficiently.[8,9] A very active area of research involves the fabrication of novel small band gap molecules possessing low-lying HOMOs with D-π-A-π-D configurations as donors for OPV.[10–16] Recently, Zeng *et al.* introduced a cyano group on the spacer of a benzothiadiazole–triphenylamine system, stabilizing the HOMO level to 5.32 eV.[10] Similarly, Cho *et al.* introduced a fluorine-substituted benzothiadiazole acceptor unit, resulting in an efficiency of 2.95%; this was due to the high V_{oc} attributed to the low HOMO level and retention of the band gap.[11] Tian and co-workers tuned the band gap of small molecules by the introduction of pyran-4-ylidenemalononitrile and the electron-donating group TPA linked by different conjugative units; an enhancement in efficiency was obtained from the compounds having low-lying HOMO values.[12] The same principle was adopted by Sassi *et al.* to control the HOMO level by synthesizing a new series of end-capped diphenylhydrazone derivatives bearing a variety of electron withdrawing conjugated bridges with different substitution patterns.[13] Romero *et al.* evaluated the band gap of the molecules by altering the acceptor strength using fluorene, fluorenone and benzothiadiazole.[14] As a result, the ICT character of the molecules were improved. Recently, Azoulay *et al.* demonstrated the tuning of HOMO–LUMO energy levels by the incorporation of various bridgehead imine-substituted cyclopentadithiophene derivatives along with the use of benzothiadiazole as a core unit; this strategy controlled the aromatic stabilization with unprecedented precision.[15]

Based on the above points, it would be of interest to develop molecules containing chromophores with high optical densities. A deliberate functional group selection for the modification of energy levels is essential so as to extend the absorption to cover the maximum range of the solar spectrum.[17] This strategy also offers the possibility to probe the structure–property relationships of the molecules and gain insight into the development of better candidates for solution-processable solar cells. Furthermore, optical and electrochemical properties could be fine-tuned by the appropriate inclusion of different π-spacers and donors into the π-conjugated backbone, which has not been extensively investigated to date.[18] In recent years, numerous articles have reported small molecule electron donors containing different heterocycle units with inherent charge transfer nature such as benzothiadiazole,[5,18] squaraines,[19] diketopyrrolopyrrole[20] and tetrazine.[21] Among these units, benzothiadiazole is considered to be one of the most versatile, and has been extensively used to make enormous improvements in organic dyes for photovoltaic applications.[22] A high efficiency of 6.8% has been reported due to the good electron carrying ability of the thiadiazole moiety. This property leads to strong π–π interactions, resulting in an ordered morphology, efficient charge transport and excellent thermal stability. The incorporation of these kinds of electron deficient moieties into the π-conjugated system stabilizes the frontier energy levels and aligns them with electron acceptor energy levels to achieve optimal efficiency with minimal loss.

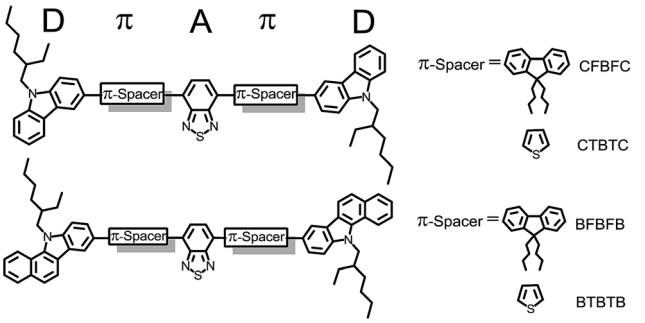

Fig. 1 Molecular structures of the dyes studied in this work.

The purpose of this combined experimental and theoretical study is to explore the absorption tuning and band gap of D-π-A-π-D conjugated backbones containing different inserted π-conjugated units with varying donor strengths. Our main design principle is to use benzothiadiazole core derivatives, which are known to yield small band gaps with benzocarbazole/carbazole donors that have low-lying HOMO levels. Herein, we report the synthesis and detailed characterization of four novel dyes based on the D-π-A-π-D architecture with benzothiadiazole as the central acceptor unit (A) and the following molecular combinations: a fluorene π-spacer with a carbazole donor (**CFBFC**) or a benzocarbazole donor (**BFBFB**) and a thiophene π-spacer with a carbazole donor (**CTBTC**) or a benzocarbazole donor (**BTBTB**) (Fig. 1). Quantum chemical calculations have been used as a guide for the analysis of the ground state and excited state properties.[23,24] The influence of π-spacers on different donors flanked with benzothiadiazole and their effects on the photophysical and electrochemical properties have been investigated for these compounds, which could help in the design of more efficient functional photovoltaic organic materials. We have compared the effects of the benzocarbazole moiety with those of its congener carbazole group as donors, along with the effects of different π-spacers. To improve the solubility and film morphology, additional ethylhexyl and butyl groups were attached to the donors and fluorene moieties, respectively.

Experimental

Materials and general procedures

Unless otherwise specified, all reactions were performed under nitrogen atmosphere using standard Schlenk techniques. All reagents were reagent/analytical grade and used without further purification. THF and toluene were distilled from sodium and benzophenone, respectively, under nitrogen atmosphere. All chromatographic separations were carried out on silica gels (60–120 mesh). ^{1}H NMR and ^{13}C NMR spectra were recorded on a Bruker Avance (300 MHz) spectrometer in $CDCl_3$ and DMSO-d_6 with TMS as a standard in both cases. Mass spectra were

obtained using electron ionization (EI) mass spectrometry (Thermofinnigan, Sanzox, CA). Gas chromatography-mass spectrometry (GCMS) was conducted on a VG70–70H, and MALDI-TOF mass spectrometry was carried out on an Axima performance MALDI-TOF/TOF mass spectrometer (Shimadzu). UV-Vis absorption spectra were measured on a Perkin-Elmer spectrofluorometer, and fluorescence spectra were recorded using a Spex model Fluorolog-3 spectrofluorometer. A Perkin-Elmer Spectrum BX spectrophotometer was used to obtain IR spectra of the dyes at a resolution of 4 cm^{-1}. Thermogravimetric analyses (TGA) were performed with a TGA/SDTA 851e (Mettler Toledo) thermal analyzer using a heating rate of 10 °C min^{-1} under nitrogen atmosphere in the temperature range of 33–550 °C. The glass-transition temperatures (T_g) of the compounds were measured using differential scanning calorimetry (DSC) under a nitrogen atmosphere at a heating rate of 10 °C min^{-1} on a DSC Q200 (TA instruments). The T_g values were determined from the second heating scan. Melting points were measured with an Electro thermal IA 9100 series digital melting point instrument and are uncorrected. Cyclic voltammetry measurements were performed on a PC-controlled CH instruments model CHI 620C electrochemical analyzer using 1 mM dye solution in dichloromethane (DCM) at a scan rate of 50 mV s^{-1}; 0.1 M tetra butyl ammonium perchlorate (TBAP) was used as a supporting electrolyte. Glassy carbon, a standard calomel electrode (SCE) and platinum wire were used as the working, reference and auxiliary electrodes, respectively.

Device fabrication and characterization of photovoltaic devices

Indium tin oxide (ITO)-coated glass (Kintek, 15 Ohms per square) was cleaned by standing in a stirred solution of 5% (v/v) Deconex 12PA detergent at 90 °C for 20 min. The ITO-coated glass was then successively sonicated for 10 min each in distilled water, acetone, and isopropanol. The substrates were then cleaned by UV/ozone at room temperature for 10 min. The UV/ozone cleaning of glass substrates was performed using a Novascan PDS-UVT UV/ozone cleaner with the platform set to maximum height. The intensity of the lamp was greater than 36 mW cm^{-2} at a distance of 10 cm. At ambient conditions, the ozone output of the UV cleaner exceeded 50 parts per million (ppm). Aqueous solutions of PEDOT/PSS (HC Starck, Baytron P AI 4083) were filtered (0.2 μm RC filter) and deposited onto glass substrates in air by spin coating (Laurell WS-400B-6NPP lite single wafer spin processor) at 5000 rpm for 60 s to give a layer with a thickness of 40 ± 5 nm. The PEDOT/PSS layer was then annealed on a hotplate in a glove box at 145 °C for 10 min. For OPV devices, the newly synthesized organic p-type materials and $PC_{61}BM$ (Nano-C) were separately dissolved in individual vials by magnetic stirring. The solutions were then combined, filtered (0.2 μm RC filter), and deposited by spin coating (SCS G3P spin coater) onto the ITO-coated glass substrates inside a glove box (with H_2O and O_2 levels both <1 ppm). Film thicknesses were determined on identical samples using a Dektak 6M Profilometer. The coated substrates were then transferred (without exposure to air) to a vacuum evaporator inside an adjacent nitrogen-filled glove box. Samples were placed on a shadow mask in a tray. The area defined by the shadow mask gave device areas of exactly 0.2 cm^2. Deposition rates and film thicknesses were monitored using a calibrated quartz thickness monitor inside the vacuum chamber. Layers of calcium (Ca; Aldrich) and aluminium (Al; 3 pellets of 99.999%; KJ Lesker) having thicknesses of 20 nm and 100 nm, respectively, were evaporated from open tungsten boats onto the active layer by thermal evaporation at pressures less than 2×10^{-6} mbar. Where used, C_{60} (Nano-C) and 2,9-dimethyl-4,7-diphenyl-1,10-phenanthroline (Aldrich) were evaporated from alumina crucibles. A connection point for the ITO electrode was made by manually scratching off a small area of the active layers. A small amount of silver paint (Silver Print II, GC Electronics, part number: 22-023) was then deposited onto all of the connection points of both ITO and Al. The completed devices were then encapsulated with glass and a UV-cured epoxy (Summers Optical, Lens Bond type J-91) by exposure to 365 nm UV light inside the glove box for 10 min. The encapsulated devices were then removed from the glove box and tested in air within 1 h. Electrical connections were made using alligator clips. The OPV devices were tested using an Oriel solar simulator fitted with a 1000 W xenon lamp filtered to give an output of 100 mW cm^{-2} at simulated AM 1.5.[25] The lamp was calibrated using a standard filtered silicon (Si) cell from Peccell Limited, which was subsequently cross-calibrated with a standard reference cell traceable to the National Renewable Energy Laboratory. The devices were tested using a Keithley 2400 source meter controlled by Labview software.

8-Bromo-11*H*-benzo[*a*]carbazole (5)

α-Tetralone (9.16 g, 6.26 mmol) and 4-bromophenylhydrazine hydrochloride (10 g, 44.7 mmol) were dissolved in 300 mL of ethanol. A catalytic amount of acetic acid was added to the reaction mixture, which was then refluxed for 3 h under nitrogen atmosphere. The reaction mixture was cooled to room temperature, and the formed product was filtered, dried and used in the next step without purification. The dried compound (9.29 g, 30.8 mmol) and tetrachloro-1-benzoquinone (10.6 g, 43.2 mmol) in *m*-xylene were refluxed under nitrogen atmosphere for 8 h and cooled to room temperature. Subsequently, NaOH (10%) and water were put into the reaction solution, and the organic layer was extracted with ethyl acetate and dried over sodium sulphate. The reaction solution was concentrated and purified by column chromatography over silica gel. The purified compound was recrystallised with ethanol to give the desired product as white crystals (8.8 g, 96% yield). ^{1}H NMR (500 MHz, $CDCl_3$): 8.24 (s, 1H), 8.23–7.99 (m, 3H), 7.68–7.44 (m, 5H). ^{13}C NMR (125 MHz, $CDCl_3$): 137.5, 132.6, 128.8, 127.0, 125.5, 125.4, 122.3, 121.6, 120.0, 119.1, 112.7. GC/MS: *m*/*z* 296 $[M]^+$.

3-Bromo-9-(2-ethylhexyl)-9*H*-carbazole (6a)

3-Bromo-9*H*-carbazole (5 g, 20.3 mmol), 2-ethylhexyl bromide (5.4 mL, 30.5 mmol), and catalytic amount of tetrabutylammonium iodide (0.75 g, 10 mol %) was taken in 50% aq. NaOH solution. The reaction mixture was continuously heated to 70 °C

for 8 h and then cooled to room temperature. The reaction mixture was extracted with hexane, washed with water and dried over anhydrous sodium sulphate. The solvent was removed under vacuum, and the crude product was purified by column chromatography over silica gel with *n*-hexane as the eluent to give the desired product as white solid (6.67 g, 92% yield). ^{1}H NMR (500 MHz, $CDCl_3$): 8.29 (s, 1H), 8.10–8.09 (d, 1H, J = 7.9 Hz), 7.63–7.57 (d, 2H, J = 8.9 Hz), 7.45–7.44 (d, 1H, d, J = 7.9 Hz), 7.35–7.32 (t, 1H, J = 14.9 Hz), 4.08–4.06 (m, 2H, N–CH_2), 2.12–2.09 (m, 1H), 1.46–1.38 (m, 8H), 1.38–0.76 (m, 6H). ^{13}C NMR (125 MHz, $CDCl_3$): 140.7, 138.9, 127.7, 125.8, 124.1, 122.4, 121.3, 119.9, 118.7, 111.1, 109.8, 108.7, 46.8, 38.8, 30.5, 28.5, 28.4, 23.9, 22.7, 13.7, 10.5. GC/MS: *m*/*z* 358 $[M]^+$.

8-Bromo-11-(2-ethylhexyl)-11*H*-benzo[*a*]carbazole (6b)

This compound was synthesized according to a procedure similar to that of **6a**, using 8-bromo-11*H*-benzo[*a*]carbazole (5.0 g, 16.9 mmol), to give the desired product as a white solid (6.4 g, 93% yield). ^{1}H NMR (500 MHz, $CDCl_3$): 8.39 (d, 1H, J = 8.3 Hz), 8.16 (d, 1H, J = 2.3 Hz), 7.99 (d, 2H, J = 8.3 Hz), 7.60–7.44 (m, 4H), 7.28 (t, 1H, J = 14.6 Hz), 4.41–4.37 (m, 2H, N–CH_2), 2.17–2.13 (m, 1H, N–CH_2–CH), 1.52–1.16 (m, 8H), 0.91–0.78 (m, 6H). ^{13}C NMR (125 MHz, $CDCl_3$): 139.6, 134.9, 133.8, 129.5, 127, 125.2, 124.8, 124.3, 122.1, 122, 121, 118.8, 118.3, 112.2, 111.2, 49.9, 39.5, 28.4, 23.8, 23, 14, 10.7. GC/MS: *m*/*z* 408 $[M]^+$.

9-(2-Ethylhexyl)-3-(4,4,5,5-tetramethyl-1,3,2-dioxaborolan-2-yl)-9*H*-carbazole (7a)

To a solution of 3-bromo-9-(2-ethylhexyl)-9*H*-carbazole (**6a**; 5 g, 14.1 mmol) in anhydrous THF (120 mL) at −78 °C, *n*-butyl lithium (2 M in hexane; 7.75 mL, 15.3 mmol) was added. The mixture was stirred at −78 °C for 2 h followed by the rapid addition of 3.25 mL of 2-isopropoxy-4,4,5,5-tetramethyl-[1,3,2]-dioxaborolane (16.7 mmol). The resulting mixture was warmed to room temperature and stirred overnight. The mixture was then poured into water and extracted with chloroform. The organic extracts were washed with brine and dried with anhydrous sodium sulphate. The solvent was removed by rotary evaporation and purified by column chromatography over silica gel with *n*-hexane : ethyl acetate (95 : 5) as the eluent to give the desired product as a white solid (5.1 g, 89% yield). ^{1}H NMR (500 MHz, $CDCl_3$): 8.64 (s, 1H), 8.12–8.10 (d, 1H, J = 8.3 Hz), 7.95–7.92 (d, 1H, J = 8.3 Hz), 7.38–7.15 (m, 4H), 3.92–3.89 (m, 2H, N–CH_2), 1.94 (m, 1H), 1.33 (s, 12H), 1.25–1.16 (m, 9H), 0.82–0.76 (t, 6H, J = 12.1). ^{13}C NMR (125 MHz, $CDCl_3$): 143.2, 141.1, 132.4, 127.9, 125.8, 123.3, 122.8, 120.6, 119.4, 109.2, 108.6, 83.6, 47.3, 39.4, 31.1, 28.9, 25.1, 24.5, 23.2, 14.3, 11.1. GC/MS: *m*/*z* 405 $[M]^+$.

11-(2-Ethylhexyl)-8-(4,4,5,5-tetramethyl-1,3,2-dioxaborolan-2-yl)-11*H*-benzo[*a*]carbazole (7b)

This compound was synthesized according to a procedure similar to that of **7a**, using 8-bromo-11-(2-ethylhexyl)-11*H*-benzo [*a*]carbazole (5.0 g, 12.3 mmol) to give the desired product as a white solid (5.3 g, 95% yield). ^{1}H NMR (500 MHz, $CDCl_3$): 8.66 (s, 1H), 8.52 (d, 1H, J = 7.9 Hz), 8.24 (d, 1H, J = 3.9 Hz), 8.02 (d, 1H, J = 6.9 Hz), 7.92 (d, 1H, J = 7.9 Hz), 7.68 (d, 1H, J = 8.9 Hz), 7.58 (m, 3H), 4.72–4.62 (m, 2H, N–CH_2), 2.28–2.24 (m, 1H, N–CH_2–CH), 1.41 (s, 12H), 1.37–1.16 (m, 8H), 0.86–0.80 (m, 6H). ^{13}C NMR (125 MHz, $CDCl_3$): 142.4, 133.8, 132.8, 130.1, 128.8, 126.4, 124.3, 123.6, 121.8, 121.6, 121.3, 120.3, 119, 118.4, 108.4, 82.7, 82.6, 49, 38.8, 29.7, 27.7, 24.3 (4-CH_3), 23, 22.2, 13.2, 10. GC/MS: *m*/*z* 455 $[M]^+$.

3-(7-Bromo-9,9-dibutyl-9*H*-fluoren-2-yl)-9-(2-ethylhexyl)-9*H*-carbazole (8a)

9-(2-Ethylhexyl)-3-(4,4,5,5-tetramethyl-1,3,2-dioxaborolan-2-yl)-9*H*-carbazole (**7a**; 4 g, 9.86 mmol), 2,7-dibromo-9,9-dibutyl-9*H*-fluorene (6; 5.17 g, 11.83 mmol) and tetrakis-(triphenylphosphine) palladium(0) (115 mg, 0.001 mmol) were dissolved in a mixture of toluene and aqueous 2 M potassium carbonate solution (3 : 1, v/v) in a round-bottomed flask equipped with a reflux condenser. The reaction mixture was heated to 80 °C for 24 h. After cooling, the reaction mixture was filtered, poured into water, extracted with chloroform and dried with anhydrous sodium sulphate. The solvent was removed by rotary evaporation and purified by column chromatography over silica gel with *n*-hexane as the eluent to give the desired product as a white foamy solid (4.6 g, 7.2 mmol, 73% yield). ^{1}H NMR (500 MHz, $CDCl_3$): 8.37 (s, 1H), 8.16–8.14 (d, 1H, J = 7.7 Hz), 7.72–7.49 (m, 4H), 7.44 (s, 1H), 7.41–7.18 (m, 7H), 4.02–4.00 (m, 2H, N–CH_2), 2.02–1.99 (m, 5H), 1.31–1.24 (m, 12H), 1.11–1.06 (m, 6H), 0.85–0.78 (m, 8H). ^{13}C NMR (125 MHz, $CDCl_3$): 153.5, 151.4, 141.9, 141.7, 140.7, 140.4, 138.7, 132.7, 130.3, 129.1, 127.6, 127.6, 126.6, 126.4, 126.2, 125.5, 123.7, 123.3, 121.8, 121.3, 121.1, 120.8, 120.5, 119.3, 119.0, 109.5, 55.7, 47.6, 40.6, 39.7, 31.3, 29.2, 26.3, 26.3, 24.7, 23.4, 14.5, 14.2, 11.3. MS (EI): *m*/*z* 635 $[M]^+$.

8-(7-Bromo-9,9-dibutyl-9*H*-fluoren-2-yl)-11-(2-ethylhexyl)-11*H*-benzo[*a*]carbazole (8b)

This compound was synthesized according to a procedure similar to that of **8a**, using 8-bromo-11-(2-ethylhexyl)-11*H*-benzo [*a*]carbazole (4.0 g, 8.79 mmol) to give the desired product as a white foamy solid (4.2 g, 6.1 mmol, 69% yield). ^{1}H NMR (500 MHz, $CDCl_3$): 8.48 (d, 1H, J = 8.3 Hz), 8.38 (d, 1H, J = 1.5 Hz), 8.23 (d, 1H, J = 9.1 Hz), 7.98 (d, 1H, J = 8.31 Hz), 7.92 (d, 1H, J = 7.9 Hz), 7.74–7.63 (m, 4H), 7.57–7.42 (m, 5H), 4.60–4.45 (m, 2H, N–CH_2), 2.27–2.22 (m, 1H, N–CH_2–CH), 2.12–1.93 (m, 4H), 1.43–1.04 (m, 8H), 0.86–0.80 (t, 6H, J = 7.55), 0.72–0.67 (t, 6H, J = 8.31). ^{13}C NMR (125 MHz, $CDCl_3$): 153.2, 151.1, 141.6, 140.8, 140.1, 138.5, 135.2, 133.8, 133.1, 130.0, 127.6, 126.4, 126.2, 125.2, 124.6, 124.3, 123.4, 122.6, 122.2, 121.6, 121.0, 120.8, 120.7, 120.1, 119.7, 119.2, 117.9, 110.2, 55.5, 50.2, 40.3, 39.7, 30.6, 28.6, 26.0, 23.9, 23.1, 14.1, 13.9, 10.8. MS (EI): *m*/*z* 684 $[M]^+$.

3-(9,9-Dibutyl-7-(4,4,5,5-tetramethyl-1,3,2-dioxaborolan-2-yl)-9*H*-fluoren-2-yl)-9-(2-ethyl hexyl)-9*H*-carbazole (9a)

To a solution of 3-(7-bromo-9,9-dibutyl-9*H*-fluoren-2-yl)-9-(2-ethylhexyl)-9*H*-carbazole (**8a**; 3 g, 4.7 mmol) in anhydrous THF (120 mL) at −78 °C, 2.6 mL of *n*-butyl lithium (2 M in hexane; 5.2 mmol) was added. The mixture was stirred at −78 °C

for 2 h. Subsequently, 2-isopropoxy-4,4,5,5-tetramethyl-[1,3,2]-dioxaborolane (1.15 mL, 5.64 mmol) was added rapidly to the solution, and the resulting mixture was warmed to room temperature and stirred overnight. The reaction mixture was poured into water and extracted with chloroform. The organic extracts were washed with brine and dried with anhydrous sodium sulphate. The solvent was removed by rotary evaporation and purified by column chromatography over silica gel with *n*-hexane : ethyl acetate (95 : 5) as the eluent to give the desired product as a white solid (2.9 g, 4.25 mmol, 90% yield). ^{1}H NMR (500 MHz, $CDCl_3$): 8.59–8.55 (d, 2H, J = 10.6 Hz), 8.37–8.34 (d, 1H, J = 8.3 Hz), 7.66–7.61 (m, 3H), 4.61 (m, 2H, N–CH_2), 2.36–2.27 (m, 5H), 1.53 (s, 12H), 1.46–1.25 (m, 12H), 0.96–0.83 (m, 16H). ^{13}C NMR (125 MHz, $CDCl_3$): 151.6, 149.7, 143.8, 141.3, 140.9, 139.9, 134.4, 133.6, 132.2, 128.5, 127.3, 126.8, 125.8, 125.4, 124.9, 123.0, 122.6, 121.1, 120.2, 120.0, 118.6, 118.3, 108.8, 108.7, 83.2, 54.8, 46.9, 40.0, 39.0, 30.6, 28.5, 26.6, 25.7, 24.6, 24.0, 22.8, 22.7, 13.8, 13.6, 10.6. ESI-MS: *m*/*z* 683 $[M]^+$.

8-(9,9-Dibutyl-7-(4,4,5,5-tetramethyl-1,3,2-dioxaborolan-2-yl)-9*H*-fluoren-2-yl)-11-(2-ethylhexyl)-11*H*-benzo[*a*]carbazole (9b)

This compound was synthesized according to the procedure similar to that of **9a**, using 8-(7-bromo-9,9-dibutyl-9*H*-fluoren-2-yl)-11-(2-ethylhexyl)-11*H*-benzo[*a*]carbazole (3.0 g, 4.38 mmol) to give the desired product as a white foamy solid. (2.8 g, 3.82 mmol, 87% yield). ^{1}H NMR (500 MHz, $CDCl_3$): 8.42–8.38 (d, 2H, J = 10.6 Hz), 8.18–8.17 (d, 1H, J = 8.3 Hz), 7.97–7.62 (m, 10H), 7.59–7.44 (m, 3H), 4.44–4.41 (m, 2H, N–CH_2), 2.12–2.09 (m, 5H), 1.36 (s, 12H), 1.29–1.08 (m, 12H), 0.82–0.79 (t, 6H), 0.70–0.66 (m, 10H). ^{13}C NMR (125 MHz, $CDCl_3$): 151.7, 149.8, 143.8, 141.3, 140.3, 139.1, 134.7, 133.6, 133.4, 132.8, 129.3, 128.6, 126.8, 125.9, 124.7, 124.2, 123.9, 122.9, 122.2, 121.9, 121.3, 120.4, 120.2, 119.3, 118.8, 118.7, 117.5, 109.8, 83.4, 54.9, 49.6, 40.1, 39.3, 30.3, 28.2, 25.7, 24.7, 23.6, 22.9, 22.7, 13.8, 13.6, 10.5. MS (EI): *m*/*z* 731 $[M]^+$.

4,7-Bis(9,9-dibutyl-7-(9-(2-ethylhexyl)-9*H*-carbazol-3-yl)-9*H*-fluoren-2-yl)benzo[*c*][1,2,5] thiadiazole (CFBFC)

3-(9,9-Dibutyl-7-(4,4,5,5-tetramethyl-1,3,2-dioxaborolan-2-yl)-9*H*-fluoren-2-yl)-9-(2-ethylhexyl)-9*H*-carbazole (**9a**; 0.98 g, 1.43 mmol) and 4,7-dibromobenzo[*c*][1,2,5]thiadiazole (200 mg, 0.7 mmol) were dissolved in a mixture of toluene and aqueous 2 M potassium carbonate solution (3 : 1, v/v). Subsequently, tetrakis(triphenylphosphine)palladium (48 mg, 0.005 mmol) and 10 mol% of 18-crown-6 were added to the solution followed by degassing with nitrogen for 15 min. The reaction mixture was heated at 80 °C under nitrogen atmosphere for 24 h. The cooled reaction mixture was filtered, poured into water, extracted with chloroform, dried over anhydrous sodium sulphate and evaporated to yield the crude product. The residue was purified by column chromatography using *n*-hexane as the eluent to give the desired product **10** as a yellow solid (658 mg, 0.53 mmol, 74% yield). ^{1}H NMR (500 MHz, $CDCl_3$): 8.42 (s, 2H), 8.22–8.20 (d, 2H, J = 7.7 Hz), 8.11–8.07 (d, 2H, J = 7.9 Hz), 7.99 (s, 2H), 7.93–7.74 (m, 8H), 7.52–7.44 (m, 3H), 7.41–7.29 (m, 6H), 7.27–7.24 (m, 3H), 4.22–4.20 (m, 2H, N–CH_2), 2.16–2.12 (m, 10H), 1.54–4.38 (m, 20H), 0.89–0.76 (m, 12H). ^{13}C NMR (125 MHz, $CDCl_3$): 154.4, 152.0, 151.3, 141.4, 141.3, 141.2, 140.4, 139.1, 135.9, 133.5, 132.6, 128.2, 127.8, 126.2, 125.7, 125.2, 123.8, 123.3, 122.9, 121.6, 120.4, 120.2, 119.6, 118.7, 109.2, 109.1, 55.3, 47.5, 40.3, 39.5, 31.0, 28.9, 26.2, 24.4, 23.2, 23.0, 14.1, 13.9, 10.9. MS (Maldi-TOF): (*m*/*z*) calcd: 1242.75; found: 1242.43.

4,7-Bis(9,9-dibutyl-7-(11-(2-ethylhexyl)-11*H*-benzo[*a*]carbazol-8-yl)-9*H*-fluoren-2-yl) benzo[*c*][1,2,5]thiadiazole (BFBFB)

This compound was synthesized according to a procedure similar to that of **10**, using 8-(9,9-dibutyl-7-(4,4,5,5-tetramethyl-1,3,2-dioxaborolan-2-yl)-9*H*-fluoren-2-yl)-11-(2-ethyl hexyl)-11*H*-benzo[*a*]carbazole (**9b**; 1.04 g, 1.43 mmol) and 2,7-dibromo benzothiadiazole (**2**) to give the desired product **11** as a yellow solid. (600 mg, 0.45 mmol, 62% yield). ^{1}H NMR (500 MHz, $CDCl_3$): 8.51–8.46 (dd, 4H, J = 22.9 Hz), 8.26–8.25 (d, 2H, J = 5.3 Hz), 8.05–8.01 (m, 5H), 7.88–7.80 (m, 5H), 7.78–7.76 (m, 3H), 7.67–7.66 (d, 2H, J = 6.4 Hz), 7.57–7.55 (d, 2H, J = 6.3 Hz), 7.52–7.51 (d, 4H, J = 8.3 Hz), 7.51–7.50 (m, 2H), 7.15 (s, 1H), 4.6–4.56 (m, 2H, N–CH_2), 2.30–2.18 (m, 10H), 1.46–1.38 (m, 24H) 1.29–1.18 (m, 19H) 0.86–0.76 (m, 12H). ^{13}C NMR (125 MHz, $CDCl_3$): 154.4, 152.0, 151.3, 141.3, 141.2, 140.7, 139.2, 135.9, 135.1, 133.7, 133.5, 129.6, 128.9, 128.2, 127.8, 126.3, 125.1, 124.5, 124.3, 123.9, 123.3, 122.5, 121.7, 120.7, 120.3, 119.6, 119.2, 117.8, 110.1, 55.3, 50.1, 40.3, 39.7, 30.6, 28.5, 26.2, 23.8, 23.2, 23.0, 14.0, 13.9, 10.8. MS (Maldi-TOF): (*m*/*z*) calcd: 1342.78; found: 1342.43.

4,7-Bis (5-(9-(2-ethylhexyl)-9*H*-carbazol-3-yl) thiophen-2-yl) benzo[*c*][1,2,5]thiadiazole (CTBTC)

A mixture of 9-(2-ethylhexyl)-3-(4,4,5,5-tetramethyl-1,3,2-dioxaborolan-2-yl)-9*H*-carbazole (**7a**; 0.93 g, 2.3 mmol) and 4,7-bis(5-bromothiophen-2-yl)benzo[*c*][1,2,5]thiadiazole (**4**; 500 mg, 1.1 mmol) was dissolved in a mixture of toluene and aqueous 2 M potassium carbonate solution (3 : 1, v/v). Subsequently, tetrakis(triphenylphosphine)palladium (63 mg, 0.005 mmol) and 18 mol% of 18-crown-6 were added to the solution, followed by degassing with nitrogen for 15 min. The reaction mixture was heated to 80 °C under nitrogen atmosphere for 24 h. The cooled crude mixture was poured into water, extracted with chloroform, dried over anhydrous sodium sulphate and evaporated to yield crude product. The residue was purified by column chromatography using *n*-hexane as the eluent to give the desired product **12** as a black solid (587 mg, 0.69 mmol, 52% yield). ^{1}H NMR (500 MHz, $CDCl_3$): 8.26 (m, 2H), 8.09–8.08 (d, 2H, J = 7.2 Hz), 7.92 (m, 2H), 7.65–7.54 (m, 6H), 7.4–7.2 (m, 8H), 3.98 (m, 4H, N–CH_2), 1.98 (m, 2H), 1.50–1.23 (m, 16H), 0.86–0.83 (m, 12H). ^{13}C NMR (125 MHz, $CDCl_3$): 152.2, 146.6, 141.1, 137.1, 128.3, 125.7, 125.1, 124.9, 124.6, 123.6, 122.9, 122.5, 122.4, 120.2, 118.8, 117.3, 117.2, 109.0, 108.9, 47.2, 30.7, 28.5, 24.1, 22.3, 13.9, 13.8, 10.7. MS (Maldi-TOF): (*m*/*z*) calcd: 854.38; found: 854.

4,7-Bis(5-(11-(2-ethylhexyl)-11*H*-benzo[*a*]carbazol-8-yl) thiophen-2-yl)benzo[*c*][1,2,5] thiadiazole (BTBTB)

This compound was synthesized according to a procedure similar to that of **12**, using 11-(2-ethylhexyl)-8-(4,4,5,5-

tetramethyl-1,3,2-dioxaborolan-2-yl)-11*H*-benzo[*a*]carbazole (**7b**; 1.04 g, 2.3 mmol) and 4,7-bis(5-bromothiophen-2-yl)benzo[*c*][1,2,5]thiadiazole (**4**) to give the desired product **13** as a brown solid (632 mg, 0.66 mmol, 59% yield). ^{1}H NMR (500 MHz, $CDCl_3$): 8.48–8.40 (m, 4H), 8.19–8.17 (m, 2H), 8.08–8.02 (m, 4H), 7.81–7.46 (m, 12H), 7.43–7.08 (m, 2H), 4.56 (m, 4H, N–CH_2), 2.23 (m, 2H), 1.55–1.24 (m, 16H), 0.86–0.84 (m, 12H). MS (Maldi-TOF): (*m*/*z*) calcd: 954.38; found: 954.

Computational details

Density functional theory (DFT) calculations were performed using the Gaussian 09 *ab initio* quantum chemical software package.[26] DFT was used to determine the ground-state properties, while time-dependent DFT (TDDFT) was employed for the estimation of ground to excited-state transitions. The optimized geometries for all the molecules in their stable conformations along with their corresponding frequencies calculated at the B3LYP/6-311G (d,p) level of theory[27–29] were used as the input for further calculations. To expedite the calculations without compromising the results, methyl groups were introduced instead of the solubilizers such as the 2-ethylhexyl group in the carbazole and benzocarbazole moieties and the two butyl groups in fluorene. The geometries were then used to obtain the frontier molecular orbitals (FMOs) and were also subjected to single-point TDDFT studies (first 15 vertical singlet–singlet transitions) to obtain the UV-Vis spectra of the dyes. The integral equation formalism polarizable continuum model (PCM)[30,31] within the self-consistent reaction field (SCRF) theory was used in the TDDFT calculations to describe the solvation of the dyes in chloroform. The TDDFT calculations were performed with various functionals including B3LYP, PBE and M06-2X. The software GaussSum 2.2.5 was employed to simulate the major portions of the absorption spectra and to interpret the nature of transitions.[32] The contribution percentages of individual units present in the dyes to the respective molecular orbitals were calculated.

Results and discussion

Synthesis of dyes

The target dyes **CFBFC**, **BFBFB**, **CTBTC** and **BTBTB** were synthesized according to a multistep synthetic pathway, as illustrated in Scheme 1. *o*-Phenylenediamine was treated with thionyl chloride to obtain benzothiadiazole (**1**), and the subsequent bromination of **1** with bromine in 47% HBr solution provided the key intermediate 4,7-dibromo benzothiadiazole (**2**).[33] Then, **2** was coupled with 2-tributylstannyl thiophene in the presence of $Pd(PPh_3)_4$ under Stille conditions to get 4,7-di(thiophen-2-yl)benzo[*c*][1,2,5]thiadiazole (**3**). Further bromination with *N*-bromosuccinimide gave 4,7-bis(5-bromo thiophen-2-l)benzo[*c*][1,2,5]thiadiazole (**4**).[34] The synthesis of 8-bromo-11*H*-benzo[*a*] carbazole (**5**) was carried out according to the Bücherer carbazole synthesis in two steps.[35] The *N*-alkylation of 3-bromo-9*H*-carbazole and 8-bromo-11*H*-benzo[*a*] carbazole by 2-ethylhexyl bromide to yield 3-bromo-9-(2-ethylhexyl)-9*H*-carbazole (**6a**) and 8-bromo-11-(2-ethylhexyl)-11*H*-benzo[*a*]carbazole (**6b**) and the C-dialkylation of 2,7-dibromofluorene by 1-bromo butane to 2,7-dibromo-9,9′-dibutyl fluorene were carried out according to modified procedures from the literature.[36] The *N*-alkylated bromo derivative of carbazole (**6a**) and benzo[*a*]carbazole (**6b**) was treated with *n*-BuLi to eliminate the halogen atoms at −78 °C, and 2-isopropoxy-4,4,5,5-tetramethyl-1,3,2-dioxaborolane was added to yield the corresponding boronate derivatives **7a** and **7b**.[37] The syntheses of bromo derivatives **8a** and **8b** were obtained in good yields by the Suzuki coupling of 2,7-dibromo-9,9′-dibutyl fluorene[38] with intermediates **7a** and **7b** in the presence of $Pd(Ph_3)_4$ as catalyst. The corresponding bromo derivatives **8a** and **8b** were again boronated by following the same procedure which is used to prepare the intermediate **7a** and **7b** and afford 3-(9,9-dibutyl-7-(4,4,5,5-tetramethyl-1,3,2-dioxaborolan-2-yl)-9*H*-fluoren-2-yl)-9-(2-ethylhexyl)-9*H*-carbazole (**9a**) and 8-(9,9-dibutyl-7-(4,4,5,5-tetramethyl-1,3,2-dioxaborolan-2-yl)-9*H*-fluoren-2-yl)-11-(2-ethylhexyl)-11*H*-benzo[*a*]carbazole (**9b**). Finally, the dyes **CFBFC** and **BFBFB** based on the fluorene π-spacer were obtained through the Suzuki coupling of **9a** and **9b**, respectively, with 4,7-dibromo benzo[*c*][1,2,5]thiadiazole (**2**), and the dyes **CTBTC** and **BTBTB** were obtained from the coupling of **8a** and **8b**, respectively, with 4,7-bis(5-bromothiophen-2-yl) benzo[*c*][1,2,5]thiadiazole (**4**) under the same reaction conditions.[39] All these molecules have been characterized by ^{1}H NMR, ^{13}C NMR, IR, and EI-MS. MALDI-TOF mass spectrometry showed molecular ions at the correct mass for the target dyes. The details of the experimental characterization data are available in the ESI.†

Molecular geometry and orbitals of the dyes

Theoretical investigation of the molecular geometries and the electron density distributions of the organic dyes was carried out to gain insight into the π-conjugated spacers and their effect on the electronic and spectroscopic properties. An important aspect to consider when assessing the degree of π-orbital overlap for efficient electron transport is the planarity of the backbone.[40] Due to the rotational freedom of the molecule, we obtain many local minima with very little difference in energy. This indicates that the molecules may not have single dominant conformations in both the solution and solid phases. To obtain a picture of the molecular orbital (MO) and vertical transitions, we froze the molecules in one local minimum and carried out further studies including TDDFT (Fig. 2).[41] Variation in the vertical transition with respect to the change in angle was investigated.

The electronic energies of the frontier molecular orbitals, which are used to assess the nature of charge transfer, and the isodensity plots of the HOMO and LUMO for the four dyes are presented in Fig. 3. The HOMO is quite delocalized all over the spacer and acceptor and, to a certain extent, on the donor part. The electron density on the terminal part of donors such as the phenyl group in carbazole and the naphthyl group in benzocarbazole is localized to a lesser extent, indicating that these moieties are not actively engaged in electron distribution, as reflected in the computed excitation energy of the dyes. The LUMO is mainly located on the central benzothiadiazole

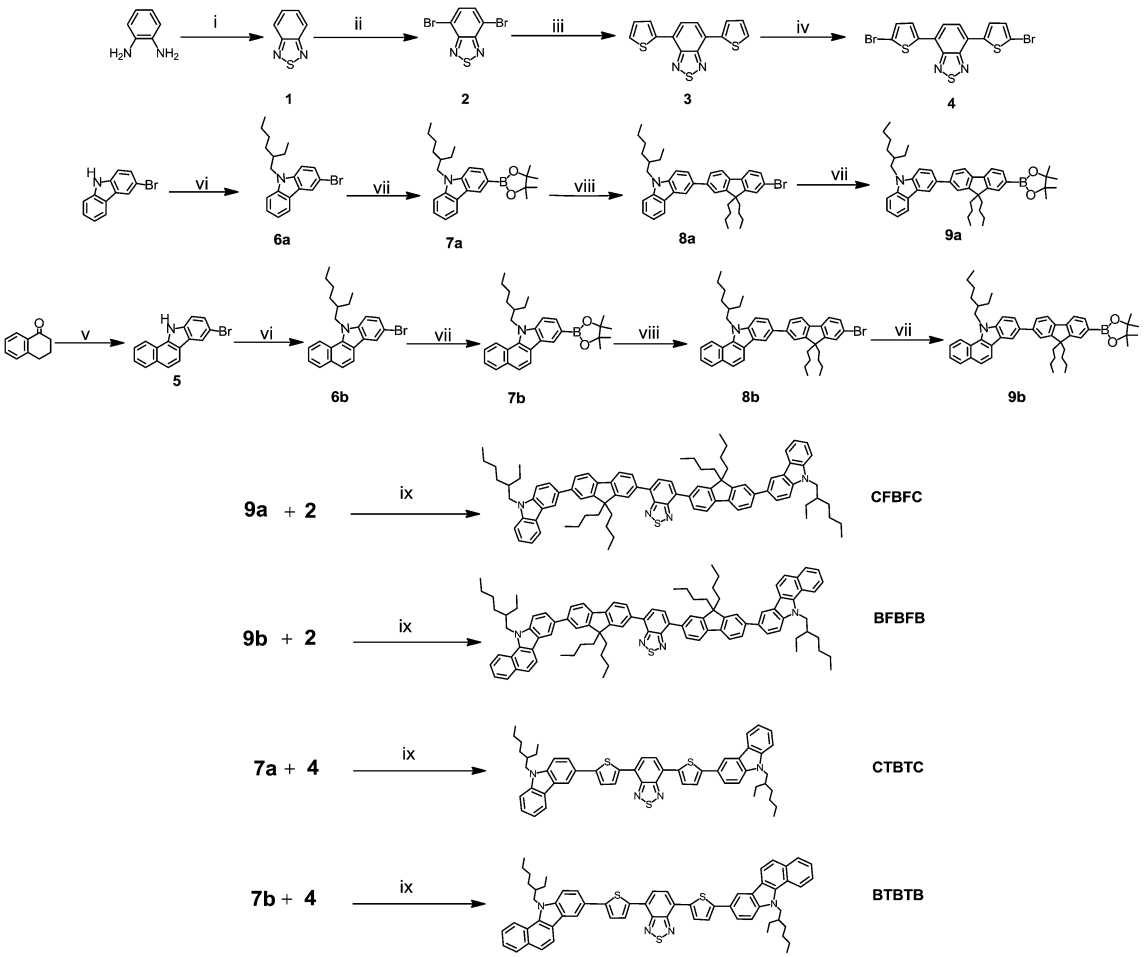

Scheme 1 Synthetic route for the preparation of target dyes. Reagents and conditions (i) $SOCl_2$, Et_3N, DCM; (ii) Br_2, 47% HBr, reflux; (iii) 2-tributylstannyl thiophene, $Pd(Ph_3)_4$, toluene; (iv) N-bromosuccinimide, $CHCl_3$, 48 h; (v) *p*-bromophenylhydrazine hydrochloride, AcOH (cat), EtOH, 80 °C; (vi) 10 mol% tetrabutyl ammonium iodide, 50% NaOH, 80 °C; (vii) *n*-BuLi, 2-isopropoxy 4,4,5,5-tetramethyl-1,3,2-dioxaborolane, THF, −78 °C, 2 h then rt; (viii) 2,7-dibromo-9,9-dibutyl-9*H*-fluorene, $Pd(Ph_3)_4$, toluene/2 M K_2CO_3; (ix) $Pd(Ph_3)_4$, 18-crown-6, toluene/2 M K_2CO_3.

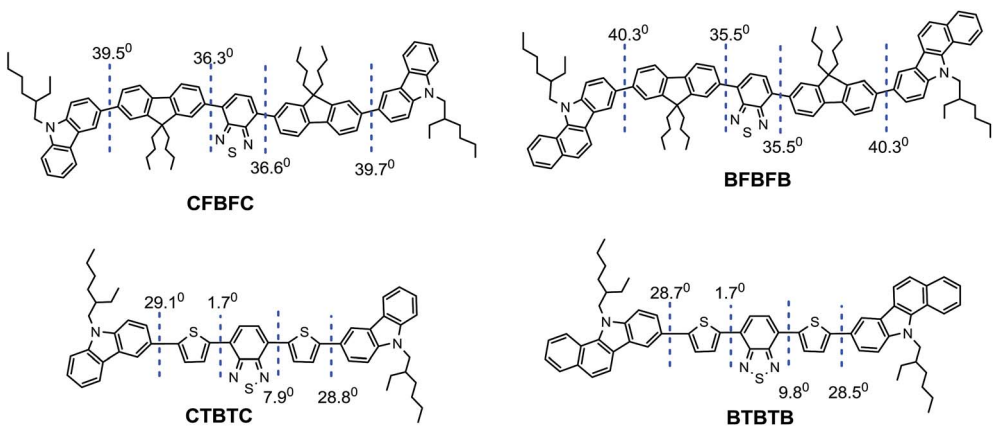

Fig. 2 Computed interplanar angles in the local ground state between the different aryl segments of the dyes.

acceptor moiety and to a lesser extent on the adjacent electron-rich thiophene rings of the thiophene derivatives. A similar pattern is also observed for the fluorene dyes. The percentage contribution of each dye segment has been computed from the frontier molecular orbitals by dividing the dyes into three segments, donor (D), π-spacer (P), and acceptor (A), using the GaussSum software. The diagram is illustrated in Fig. S3, ESI.†

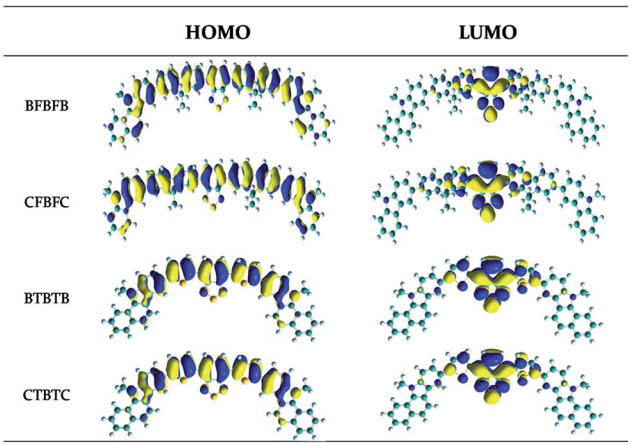

Fig. 3 Computed isodensity (0.02) surfaces of the HOMO and LUMO of the target molecules.

Optical properties

The evaluation of optical properties is essential to understand the applicability of small molecules for optoelectronic devices. Fig. 4 depicts the UV-Visible absorption and emission spectra of the four dyes **CFBFC**, **BFBFB**, **CTBTC** and **BTBTB** in chloroform solution; the corresponding optical properties are compiled in Table 1. All the compounds exhibited two absorption bands characteristic of donor–acceptor based systems. Among them, the higher energy absorption band at 320–370 nm corresponds to the localized π–π* transition of the conjugated backbone. The intensity of the π–π* transition peaks for the fluorene dyes are relatively high. Dyes based on fluorene π-spacers such as **CFBFC** and **BFBFB** display the lower energy absorption band at 382–516 nm with a molar extinction coefficient of $\sim 3.5 \times 10^4$ M^{-1} cm^{-1}, which is ascribed to the intramolecular charge transfer (ICT) transition from the donor segments to the acceptor group.[42–44] The longer wavelength absorption maxima of 433 nm in **BFBFB**, which has benzocarbazole as the donor, is almost identical to that of **CFBFC** (434 nm), its carbazole counterpart. This indicates that the introduction of different types of donors such as carbazole and benzocarbazole has a less pronounced effect on the ICT for fluorene-based dyes. It is important to note that, in comparison to the absorption spectra of fluorene-based analogues, compounds based on a thiophene π-spacer such as **CTBTC** and **BTBTB** exhibit two distinct absorption maxima at 524 nm and 499 nm, respectively. The substitution of thiophene in place of fluorene leads to a 65–90 nm bathochromic shift in both the absorption and emission profiles. Additionally, the dye **BTBTB**, which contains benzocarbazole as a donor, displays hyperchromic and hypsochromic effects when compared to **CTBTC**.[45] It has been noted that the area of the ICT band of thiophene dyes (~250 nm) is almost two times as broad as that of fluorene dyes (~136 nm); the intensity is also comparatively high, which implies that the ICT characters of the dyes are enhanced by replacing the fluorene spacer units with thiophene. In the film state, the absorption spectra exhibit an apparent broadening and bathochromic shift of absorption bands corresponding to those of the solution spectra due to the well-structured and intermolecular interactions in the solid state.[46] Thus, the replacement of fluorene π-spacers with thiophene leads to: (1) a considerable reduction in band gap with a large extension in spectral response, indicating that thiophene as a π-spacer provides effective electronic communication between donor and acceptor; and (2) the extensive delocalization of thiophene dyes, leading to a bathochromic shift due to the more planar conformation and high-lying π-orbital along with the smaller aromatic resonance energy of the thiophene entity compared to fluorene.[47,48]

To further investigate the effect of solvent–solute interactions on the ICT character of the dyes, absorption spectra were recorded in various solvents. The UV-Vis absorption and emission spectra of **CTBTC** recorded in various solvents are shown in Fig. 5, and the spectra of the remaining dyes are shown in ESI.† All the dyes showed negligible response to solvent polarity for intramolecular charge-transfer in the ground state.[49] In contrast, the emission spectra of the dyes red shifted remarkably as the solvent polarity increased. Thus, it is clear that in the presence of polar solvent, the non-polar locally excited (LE) state observed in absorption is transformed into a polar excited state as seen in emission.[50] A distinct solvatochromic effect is observed for the thiophene derivatives in contrast to the

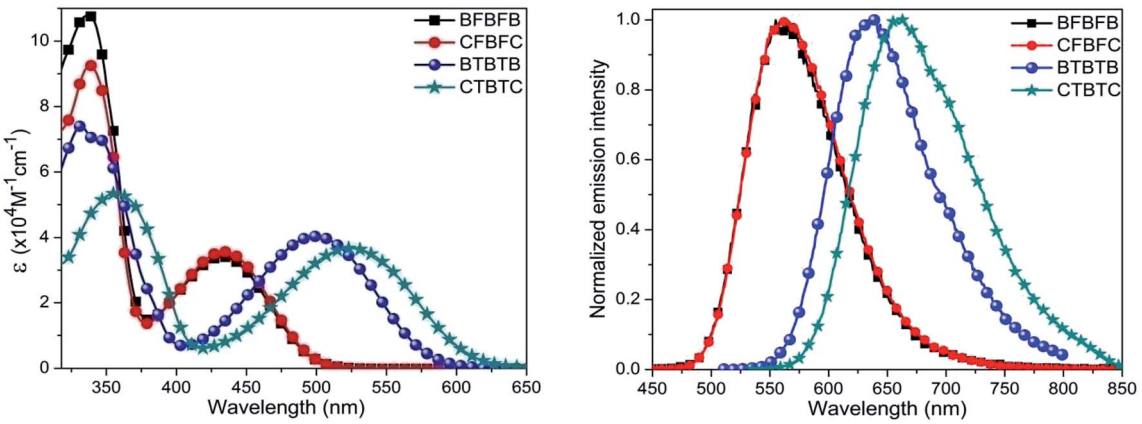

Fig. 4 UV-Vis absorption and emission spectra of dyes recorded in chloroform.

Table 1 Optical properties and thermal analysis data of the dyes[a]

Dye	λ_{abs}[b] (nm)	ε (M^{-1} cm^{-1})	λ_{flu}[b] (nm)	λ_{abs}[c] film	Stokes shift (cm^{-1})	$E_{g,opt}$[d] (eV)	T_d (°C)	T_m (°C)	T_g (°C)
BFBFB	433	34 063	563	447	5333	2.36	433	270	121
	337	107 859							
CFBFC	434	35 653	563	447	5280	2.30	435	215	98
	338	92 477							
BTBTB	499	40 343	639	521	4391	1.95	376	192	96
	332	74 029							
CTBTC	524	36 706	663	544	4001	1.85	372	173	63
	356	53 401							

[a] T_d – decomposition temperature (corresponding to 5% weight loss). T_m – melting point of the compounds. T_g – glass transition temperature; values are from the second heating scan. [b] Absorption and emission spectra in chloroform at a concentration of 1×10^{-5} M at ambient temperature. [c] Measured in thin film state. [d] Estimated from the onset absorption spectra of the compounds in thin film state.

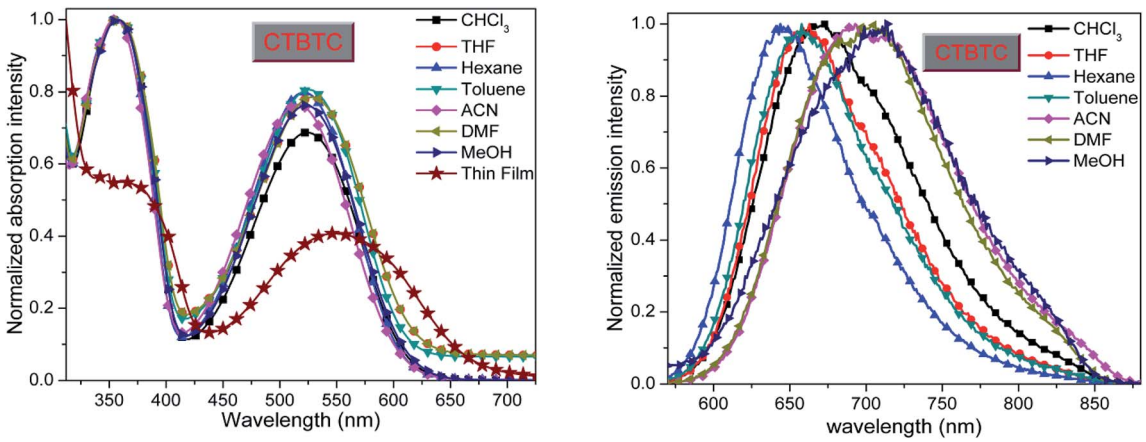

Fig. 5 Solvatochromism observed from UV-Vis absorption and emission spectra of **CTBTC** recorded in various solvents (for remaining dyes see ESI†).

fluorene dyes. For example, the emission maximum λ_{max} of **CTBTC** is red-shifted from 644 nm in hexane to 712 nm in DMF, which implies that the excited state of the compound is well stabilized upon an increase in solvent polarity, resulting in the red shifted emission. The large Stokes shifts observed for the fluorene dyes reveal that these dyes undergo more structural relaxation during photoexcitation.[51] The optical band gap (E_g) (Table 1) was derived from the onset absorption spectra of the dyes in thin film state.

Based on the experimental observations, TDDFT studies of these molecules were carried using different energy functionals (B3LYP, PBE and M06-2X) with the 6-311G (d,p) basis set in order to gain a deeper understanding of the excited-state transitions.[52,53] The transition energies obtained in the gas phase using the B3LYP and PBE functionals are highly overestimated compared to the experimental results. On the other hand, the gas phase absorption spectra results computed using M06-2X show only a small underestimation; thus, this functional was further used in the framework of the polarizable continuum model (PCM) with chloroform as the solvent. These results are in reasonable agreement with the experimental values. Table 2 contains the computed vertical excitations along with the oscillator strengths, frontier orbital energies and compositions of vertical transitions in terms of molecular orbitals for all the dyes. The ground state and transition dipole moments of the dyes computed from DFT and TDDFT calculations also corroborate the experimental observations. The intramolecular charge transfer excited state is clearly formed from the HOMO to LUMO transition. The percentage contribution of thiophene as a π-spacer is superior to that of fluorene with regard to the electronic properties of the molecule, which may be attributed to the effective orbital mixing over the whole π-conjugated system (Fig. S3, ESI†).[8b]

To ascertain the charge transfer nature of the π-spacers of the dyes upon photoexcitation, we performed absorption studies as a function of dihedral angle. This was done by varying the dihedral angle between the donor *vs.* π-spacer and π-spacer *vs.* acceptor in both the fluorene and thiophene derivatives from 0° to 60° in steps of 5° using TDDFT calculations.[54,55] The structures used for these calculations were obtained from the optimized geometries at the B3LYP/6-311G (d,p) level. The absorption values obtained for these two derivatives with different positions are plotted against dihedral angle in ESI (Fig. S5 and S6†). The figures clearly show that the deviation of dihedral angle between the donor and π-spacer has a pronounced effect on the absorption of **BTBTB**, leading to a 45

Table 2 Comparison of the experimental optical properties with the theoretical data

		M06-2X (chloroform)				
Dye	λ_{max}[a] (nm)	λ_{max} (nm)	f (oscillation strength)	Composition	μ_{gs}[b]	μ_{ge}[c]
BFBFB	433	404 (3.07 eV)	1.61	HOMO → LUMO (54%), HOMO-2 → LUMO (25%)	2.3	2.6
CFBFC	434	404 (3.07 eV)	1.54	HOMO → LUMO (65%), HOMO-2 → LUMO (25%)	2.1	2.5
BTBTB	499	500 (2.48 eV)	1.37	HOMO → LUMO (90%), HOMO-2 → LUMO (5%)	2.3	3.1
CTBTC	524	503 (2.47 eV)	1.19	HOMO → LUMO (92%), HOMO-2 → LUMO (4%)	2.3	3.1

[a] Recorded in chloroform (1×10^{-5} M solution). [b] Dipole moment of the dyes in the ground state (debye units) obtained from the B3LYP/6-311G (d,p) level. [c] Transition dipole moment of the dyes (debye units) obtained from the M06-2X/6-311G (d,p) level.

nm bathochromic shift; in contrast, only an 11 nm redshift is observed in the case of **BFBFB**. The dye **BTBTB** exhibits a four-fold variation in absorption, substantiating the idea that the thiophene as a π-bridge unit promotes efficient electron transport over the entire molecule. The variations in absorption in terms of dihedral angle deviation between the spacer and acceptor for these molecules are almost the same (~97 nm).

Electrochemical studies

In order to evaluate the electrochemical properties of these dyes, the redox behavior was investigated by performing cyclic voltammetry (CV) using a standard three-electrode configuration.[54] The oxidation potentials in the voltammograms reveal that all compounds undergo irreversible oxidation (Fig. 6). The HOMO levels of all the dyes were calculated from the onset oxidation potential according to the empirical formula $E_{HOMO} = -e(E_{ox} + 4.4)$ (eV), and the LUMO levels were estimated from the onset reduction potentials[55] according to the empirical formula $E_{LUMO} = -e(E_{red} + 4.4)$ (eV); the calculation results are compiled in Table 3. The onset oxidation potentials of the fluorene dyes **BFBFB** and **CFBFC** and the thiophene dyes **BTBTB** and **CTBTC** are estimated to be 1.35 V, 1.27 V, 1.13 V and 0.92 V, corresponding to HOMO levels of −5.75 eV, −5.67 eV, −5.53 eV, and −5.32 eV, respectively. Among these compounds, **BFBFB** and **BTBTB** show more positive shifts in oxidation potential, implying that the incorporation of the benzocarbazole moiety has a significant lowering effect on the HOMO level compared to that of the carbazole counterpart. This effect should also improve the V_{oc} because V_{oc} is proportional to the energy difference between the HOMO of the electron donor and the LUMO of the electron acceptor in small molecule organic solar cells.[45b] The onset reduction potentials of **BFBFB**, **CFBFC**, **BTBTB** and **CTBTC** are estimated to be −1.12 V, −1.17 V, −0.95 V and −0.97 V, corresponding to LUMO levels of −3.28 eV, −3.23 eV, −3.45 eV and −3.43 eV, respectively. The introduction of thiophene as a π-spacer in place of fluorene leads to a reduction in the band gap, and the HOMO and LUMO levels shift upwards and downwards by 0.22 eV and 0.17 eV, respectively, for **BTBTB** compared to **BFBFB** and 0.35 eV and 0.19 eV, respectively, for **CTBTC** compared to **CFBFC** (Fig. 7). The band gap is reduced in the following order: **BFBFB** (2.47 eV) > **CFBFC** (2.44 eV) > **BTBTB** (2.08 eV) > **CTBTC** (1.90 eV). The HOMO–LUMO gaps (ΔE) derived from cyclic voltammetry (CV) are in good agreement with the optical band gaps determined from the onset absorption spectra in the thin film state. The DFT calculated HOMO/LUMO energies are −5.25 eV/−2.55 eV and −5.24 eV/−2.53 eV for the fluorene derivatives and −5.00 eV/−2.67eV and −4.97/−2.66 for the thiophene derivatives. The HOMO–LUMO gaps calculated from the frontier orbital energy values are estimated to be 2.7 eV for the fluorene derivatives and 2.32–2.33 eV for the thiophene derivatives. These values are in reasonably good agreement with the estimated electrochemical and optical band gap data. Band gaps calculated using hybrid functionals with fully periodic boundary conditions (PBC) usually give better agreement with experimental results.[56]

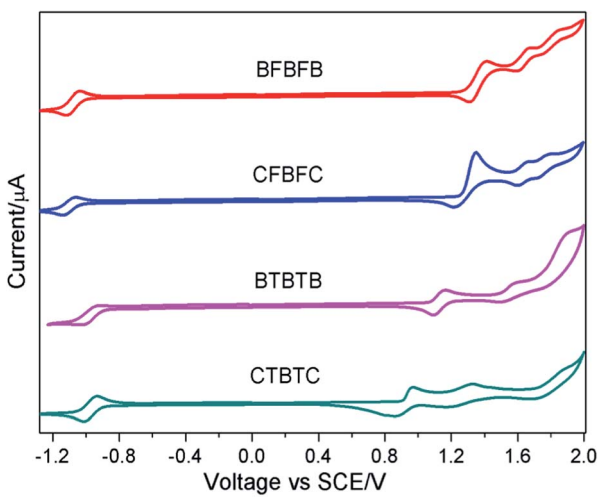

Fig. 6 Cyclic voltammograms of the dyes recorded in DCM.

Thermal properties

The TGA analysis depicted in Fig. 8 reveals that the 5% weight loss temperatures (T_d) of the dyes range from 372–433 °C. The T_g and T_m values of the benzocarbazole dyes are comparatively higher than those of the carbazole dyes, as seen in Fig. 9 and

Table 3 Comparison of electrochemical measurements *vs.* values obtained from DFT

	E_{onset}[a] (V)					DFT[d]		
Dye	Oxd	Red	HOMO[b] (eV)	LUMO[b] (eV)	$E_{g,ele}$[c] (eV)	HOMO (eV)	LUMO (eV)	Band gap[e] (eV)
BFBFB	1.35	−1.12	−5.75	−3.28	2.47	−5.25	−2.55	2.70
CFBFC	1.27	−1.17	−5.67	−3.23	2.44	−5.24	−2.53	2.70
BTBTB	1.13	−0.95	−5.53	−3.45	2.08	−5.00	−2.67	2.33
CTBTC	0.92	−0.97	−5.31	−3.43	1.90	−4.97	−2.66	2.32

[a] Measured in CH_2Cl_2 with 0.1 M tetrabutylammonium perchlorate (TBAPC) as a supporting electrolyte with a scan rate of 50 mV s^{-1}. [b] Deduced from the formulas HOMO = −(4.4 + E_{ox}) and LUMO = −(4.4 + E_{red}). [c] Bandgap obtained from electrochemical data. [d] Computed values from the B3LYP/6-311G (d,p) level. [e] Band gap obtained from theoretical data.

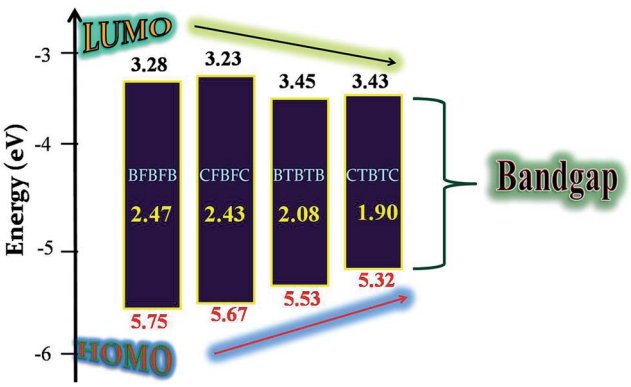

Fig. 7 Schematic representation of the band gap reductions estimated from the electrochemical data.

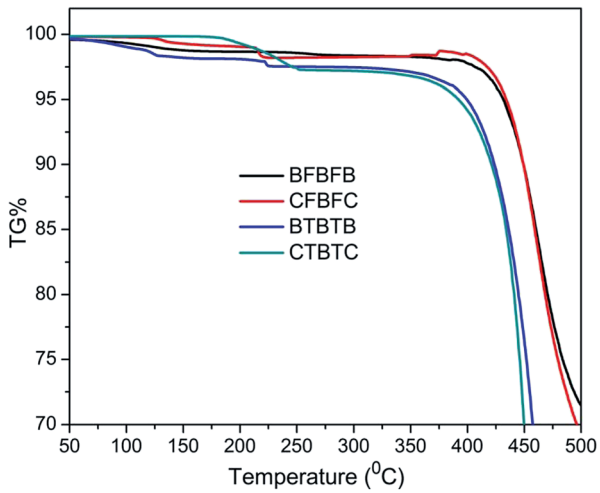

Fig. 8 TGA thermograms measured at a heating rate of 10 °C min^{-1} under N_2 atmosphere.

Table 1. The T_g values determined from the second heating scan range from 63–124 °C. It is apparent that the fluorene analogues exhibit greater thermal stability than their thiophene counterparts due to the presence of the rigid structural fluorene units.[57] All the dyes have good thermal stability, which is essential for device fabrication processes and other types of applications.

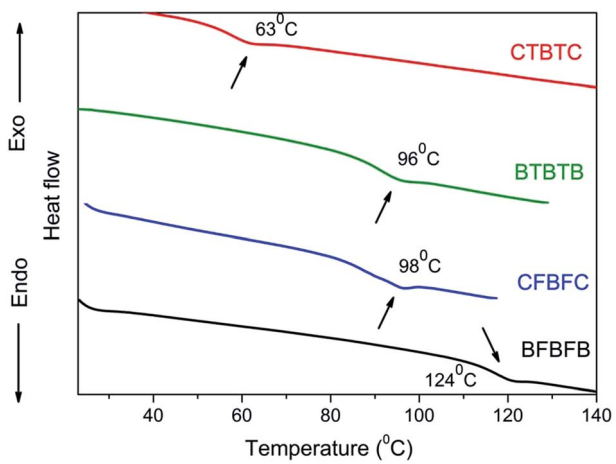

Fig. 9 DSC traces of the dyes recorded at a heating rate of 10 °C min^{-1}.

Photovoltaic properties

Because of their appropriate optoelectronic features, solubilities and good film-forming capabilities, all the synthesized dyes were incorporated as p-type semiconducting components with the soluble fullerene derivative [6,6]-phenyl-C_{61}-butyric acid methyl ester ($PC_{61}BM$) as an n-type semiconductor in bulk-heterojunction (BHJ) photovoltaic devices. BHJ architectures typically deliver higher device power conversion efficiencies by maximizing the surface area of the interface between the donor and acceptor materials in the active layer. For all the compounds, the device structure used was ITO/PEDOT:PSS (38 nm)/active layer/Ca (20 nm)/Al (100 nm), where the active layer was a solution-processed blend of one of the donor materials reported here and the solubilised fullerene $PC_{61}BM$. The active layers were prepared by spin coating mixtures of the appropriate dye with $PC_{61}BM$ in chlorobenzene under ambient conditions in 1 : 1 ratios without subsequent annealing. The optimum layer thickness was found to be in the range of approximately 70 nm. The best photovoltaic devices based on **CTBTC** gave a power conversion efficiency (η) of 1.62%. The respective current–voltage (J–V) curves are shown in Fig. 10.

The relatively lower efficiency achieved with **BFBFB, CFBFC** and **BTBTB** compared to **CTBTC** is likely due to the weaker absorption of the visible spectrum. This suggests that the light

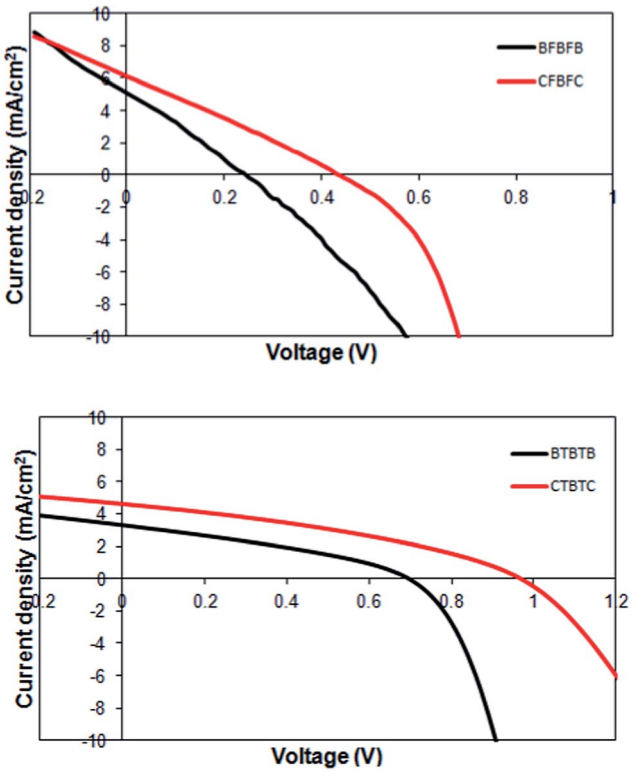

Fig. 10 Characteristic current density *versus* voltage (*J*–*V*) curves for the best BHJ devices based on **BFBFB** & **CFBFC** (upper) and **BTBTB** & **CTBTC** (lower) in blends with $PC_{61}BM$ under simulated sunlight (100 mW cm^{-2}, AM 1.5G). The device structure is: ITO/PEDOT:PSS (38 nm)/active layer/Ca (20 nm)/Al (100 nm).

harvesting ability of the small molecule donors plays an important role in achieving their optimum photovoltaic performance. The modest fill factors observed for all devices suggest that the pathways for charge to be carried to the electrodes are not optimized, a problem that could be addressed by using donor fragments that encourage stronger intermolecular interactions. In regard to the processing conditions of the blend solutions, previous studies[58] indicate that the solvent and degree of crystallization have a strong effect on cell performance. Our attempts to fabricate the devices using a low-boiling-point solvent such as chloroform resulted in very poor photovoltaic performance, primarily due to poor film quality. The finding that the OPV devices comprised of these novel donor materials perform better with high-boiling-point solvents is significant as the use of high-boiling-point solvents is preferable from a processing point of view. Table 4 presents the comparative photovoltaic performance data.

This preliminary study was conducted using a C_{60}-derivative of PCBM; however, reports using a C_{70}-derivative for efficiency enhancement mainly attribute the results to the enhanced absorption in the film. These latter derivatives might be useful for device optimization using the materials reported in this work; this will be studied in the near future.

Conclusion

In summary, we have reported four benzothiadiazole core-structured compounds based on D-π-A-π-D architecture featuring different π-spacers (fluorene and thiophene) along with benzocarbazole and carbazole as donors. The significance of these modifications on the individual segments of the dyes was thoroughly investigated using a range of experimental techniques including optical, electrochemical and thermal methods. The enhanced oxidative and thermal stability of **BFBFB** and **BTBTB** indicate that the benzocarbazole functionality can play a vital role as a donor for optoelectronic applications. The substitution of thiophene as a π-spacer in place of fluorene has a pronounced effect on the photophysical and electrochemical properties of the dyes. The electrochemical bandgaps of these dyes are greatly reduced by changing the π-spacer from fluorene to thiophene and are in good agreement with the band gap data derived from with the band gap data derived from optical methods. From the electronic structures calculated by DFT methods, it is clear that the better performance of thiophene as a π-spacer is largely due to the planarity of the molecule. The results obtained from thermal methods clearly establish that all the dyes have high decomposition temperatures (T_d) in the range of 372–435 °C. The significant electronic and optical properties demonstrated by these dyes allowed us to fabricate them in solution-processable BHJ OPV devices. After preliminary device examination, the devices with **CTBTC** as the donor material exhibited the best efficiency (1.62%) with $PC_{61}BM$. The inferior performance observed for the remaining materials is likely related to their weaker absorption in the visible region. Our results not only enrich the molecular library of donors, but also highlight the importance of considering factors such as (1) light-harvesting, (2) charge carrier mobility and (3) solvent selection when designing small-molecule donors. Further examination of device fabrication using C_{70}-derivatives of PCBM is the subject of on-going work in our laboratories.

Table 4 Comparative BHJ solar cell performances

Dye	Blend film thickness[a] (1 : 1@3000 rpm)	V_{oc} (mV)	J_{sc} (mA cm^{-2})	FF	Efficiency[b] (η%)
BFBFB	64	250 ± 30	5.09 ± 0.4	0.23 ± 0.04	0.30 ± 0.08
CFBFC	66	430 ± 20	6.13 ± 0.6	0.26 ± 0.03	0.71 ± 0.15
BTBTB	62	691 ± 30	3.30 ± 0.3	0.32 ± 0.02	0.76 ± 0.07
CTBTC	63	960 ± 20	4.63 ± 0.2	0.34 ± 0.03	1.62 ± 0.06

[a] BHJ devices with specified weight ratios. The device structure is ITO/PEDOT:PSS (38 nm)/active layer/Ca (20 nm)/Al (100 nm) with an active layer thickness of approximately 65 nm. [b] Average value based on 10 devices.

Acknowledgements

MP thanks UGC for the fellowship. We thank the director of CSIR-IICT for the encouragement. We acknowledge funding from the NWP-0054 project. SVB acknowledges the Australian Research Council under a Future Fellowship Scheme (FT110100152) and the School of Applied Sciences (RMIT University) for providing the facilities.

References

1 (*a*) Y. J. Cheng, S. H. Yang and C. S. Hsu, *Chem. Rev.*, 2009, **109**, 5868–5923; (*b*) B. C. Thompson and J. M. J. Fréchet, *Angew. Chem., Int. Ed.*, 2008, **47**, 58–77; (*c*) C. Duan, F. Huang and Y. Cao, *J. Mater. Chem.*, 2012, **22**, 10416; (*d*) Y. Li, *Acc. Chem. Res.*, 2012, **45**, 723–733.

2 (*a*) P. Heremans, D. Cheyns and B. P. Rand, *Acc. Chem. Res.*, 2009, **42**, 1740–1747; (*b*) R. Kroon, M. Lenes, J. C. Hummelen, P. W. M. Blom and B. De Boer, *Polym. Rev.*, 2008, **48**, 531–582; (*c*) E. Bundgaard and F. C. Krebs, *Sol. Energy Mater. Sol. Cells*, 2007, **91**, 954–985; (*d*) C. L. Chochos and S. A. Choulis, *Prog. Polym. Sci.*, 2011, **36**, 1326–1414; (*e*) N. Blouin and M. Leclerc, *Acc. Chem. Res.*, 2008, **41**, 1110–1119.

3 (*a*) A. Mishra and P. Bäuerle, *Angew. Chem., Int. Ed.*, 2012, **51**, 2020–2068; (*b*) Y. Lin, Y. Li and X. Zhan, *Chem. Soc. Rev.*, 2012, **41**, 4245–4272; (*c*) B. Walker, C. Kim and T. Q. Nguyen, *Chem. Mater.*, 2011, **23**, 470–482.

4 (*a*) Y. Chen, X. Wan and G. Long, *Acc. Chem. Res.*, 2013, **46**, 2645–2655; (*b*) F. Zhang, D. Wu, Y. Xu and X. Feng, *J. Mater. Chem.*, 2011, **21**, 17590; (*c*) Z. B. Henson, K. Müllen and G. C. Bazan, *Nat. Chem.*, 2012, **4**, 699–704; (*d*) J. E. Coughlin, Z. B. Henson, G. C. Welch and G. C. Bazan, *Acc. Chem. Res.*, 2014, **47**, 257–270.

5 (*a*) J. Zhou, Y. Zuo, X. Wan, G. Long, Q. Zhang, W. Ni, Y. Liu, Z. Li, G. He, C. Li, B. Kan, M. Li and Y. Chen, *J. Am. Chem. Soc.*, 2013, **135**, 8484–8487; (*b*) J. Zhou, Y. Zuo, X. Wan, Y. Liu, Y. Zuo, Z. Li, G. He, G. Long, W. Ni, C. Li, X. Su and Y. Chen, *J. Am. Chem. Soc.*, 2012, **134**, 16345–16351; (*c*) T. S. Van der Poll, J. A. Love, T. Q. Nguyen and G. C. Bazan, *Adv. Mater.*, 2012, **24**, 3646–3649; (*d*) A. K. K. Kyaw, D. H. Wang, V. Gupta, J. Zhang, S. Chand, G. C. Bazan and A. J. Heeger, *Adv. Mater.*, 2013, **25**, 2397–2402.

6 http://www.heliatek.com/newscenter/latest_news/neuer-weltrekord-fur-organische-solarzellen-heliatek-behauptet-sich-mit-12-zelleffizienz-als-technologiefuhrer/?lang=en.

7 (*a*) H. Spanggaard and F. C. Krebs, *Sol. Energy Mater. Sol. Cells*, 2004, **83**, 125–146; (*b*) J. L. Bŕedas, J. E. Norton, J. Cornil and V. Coropceanu, *Acc. Chem. Res.*, 2009, **42**, 1691–1699; (*c*) J. Roncali, *Chem. Rev.*, 1997, **97**, 173–205.

8 (*a*) L. Pandey, C. Risko, J. E. Norton and J. L. Breédas, *Macromolecules*, 2012, **45**, 6405–6414; (*b*) K. Takimiya, I. Osaka and M. Nakano, *Chem. Mater.*, 2014, **26**, 587–593; (*c*) E. Kozma and M. Catellani, *Dyes Pigm.*, 2013, **98**, 160–179.

9 C. He, Q. He, X. Yang, G. Wu, C. Yang, F. Bai, Z. Shuai, L. Wang and Y. Li, *J. Phys. Chem. C*, 2007, **111**, 8661–8666.

10 S. Zeng, L. Yin, C. Ji, X. Jiang, K. Li, Y. Li and Y. Wang, *Chem. Commun.*, 2012, **48**, 10627–10629.

11 N. Cho, K. Song, J. K. Lee and J. Ko, *Chem.–Eur. J.*, 2012, **18**, 11433–11439.

12 Z. Li, J. Pei, Y. Li, B. Xu, M. Deng, Z. Liu, H. Li, H. Lu, Q. Li and W. Tian, *J. Phys. Chem. C*, 2010, **114**, 18270–18278.

13 M. Sassi, M. Crippa, R. Ruffo, R. Turrisi, M. Drees, U. K. Pandey, R. Termine, A. Golemme, A. Facchetti and L. Beverina, *J. Mater. Chem. A*, 2013, **1**, 2631–2638.

14 J. R. Romero, L. A. Ixta, M. Rodríguez, G. R. Ortíz, J. L. Maldonado, A. J. Sánchez, N. Farfán and R. Santillan, *Dyes Pigm.*, 2013, **98**, 31–41; S. Tang, B. Li and J. Zhang, *J. Phys. Chem. C*, 2013, **117**, 3221–3231.

15 J. D. Azoulay, Z. A. Koretz, B. M. Wong and G. C. Bazan, *Macromolecules*, 2013, **46**, 1337–1342.

16 (*a*) Y. Liu, Y. M. Yang, C. Chen, Q. Chen, L. Dou, Z. Hong, G. Li and Y. Yang, *Adv. Mater.*, 2013, **25**, 4657–4662.

17 A. Marrocchi, F. Silvestri, M. Seri, A. Facchetti, A. Taticchi and T. J. Marks, *Chem. Commun.*, 2009, 1380–1382.

18 (*a*) B. A. D. Neto, A. A. M. Lapis, E. N. S. Júnior and J. Dupont, *Eur. J. Org. Chem.*, 2013, **2**, 228–255; (*b*) S. Xue, S. Liu, F. He, L. Yao, C. Gu, H. Xu, Z. Xie, H. Wu and Y. Ma, *Chem. Commun.*, 2013, **49**, 5730–5732.

19 (*a*) L. Beverina and P. Salice, *Eur. J. Org. Chem.*, 2010, 1207–1225; (*b*) L. Beverina, M. Drees, A. Facchetti, M. Salamone, R. Ruffo and G. A. Pagani, *Eur. J. Org. Chem.*, 2011, 5555–5563; (*c*) F. Silvestri, M. D. Irwin, L. Beverina, A. Facchetti, G. A. Pagani and T. J. Marks, *J. Am. Chem. Soc.*, 2008, **130**, 17640–17641; (*d*) D. Bagnis, L. Beverina, H. Huang, F. Silvestri, Y. Yao, H. Yan, G. A. Pagani, T. J. Marks and A. Facchetti, *J. Am. Chem. Soc.*, 2010, **132**, 4074–4075.

20 (*a*) S. Qu and H. Tian, *Chem. Commun.*, 2012, **48**, 3039–3051; (*b*) B. Walker, A. B. Tamayo, X. D. Dang, P. Zalar, J. H. Seo, A. Garcia, M. Tantiwiwat and T. Q. Nguyen, *Adv. Funct. Mater.*, 2009, **19**, 3063–3069.

21 (*a*) Y. Chen, C. Li, P. Zhang, Y. Li, X. Yang, L. Chen and Y. Tu, *Org. Electron.*, 2013, **14**, 1424–1434; (*b*) Z. Li, J. Ding, N. Song, J. Lu and Y. Tao, *J. Am. Chem. Soc.*, 2010, **132**, 13160–13161.

22 (*a*) L. Lin, Y. Chen, Z. Huang, H. Lin, S. Chou, F. Lin, C. Chen, Y. Liu and K. Wong, *J. Am. Chem. Soc.*, 2011, **133**, 15822–15825; (*b*) Y. Chen, L. Lin, C. Lu, F. Lin, Z. Huang, H. Lin, P. Wang, Y. Liu, K. T. Wong, J. Wen, D. J. Miller and S. B. Darling, *J. Am. Chem. Soc.*, 2012, **134**, 13616–13623.

23 (*a*) N. Metri, X. Sallenave, C. Plesse, L. Beouch, P. H. Aubert, F. Goubard, C. Chevrot and G. Sini, *J. Phys. Chem. C*, 2012, **116**, 3765–3772; (*b*) J. Zapala, M. Knor, T. Jaroch, A. M. Niedbala, E. Kurach, K. Kotwica, R. Nowakowski, D. Djurado, J. Pecaut, M. Zagorska and A. Pron, *Langmuir*, 2013, **29**, 14503–14511; (*c*) L. Sun, F. Bai, Z. Zhao and H. Zhang, *Sol. Energy Mater. Sol. Cells*, 2011, **95**, 1800–1810.

24 (*a*) N. M. O'Boyle, C. M. Campbell and G. R. Hutchison, *J. Phys. Chem. C*, 2011, **115**, 16200–16210; (*b*) S. Tang and J. Zhang, *J. Comput. Chem.*, 2012, **33**, 1353–1363; (*c*) Y. Duan, Y. Geng, H. Li, J. Jin, Y. Wu and Z. Su, *J. Comput. Chem.*, 2013, **34**, 1611–1619.

25 A. Gupta, A. Ali, A. Bilic, M. Gao, K. Hegedus, B. Singh, S. E. Watkins, G. J. Wilson, U. Bach and R. A. Evans, *Chem. Commun.*, 2012, **48**, 1889–1891.

26 M. J. Frisch, G. W. Trucks, H. B. Schlegel, G. E. Scuseria, M. A. Robb, J. R. Cheeseman, G. Scalmani, V. Barone, B. Mennucci and G. A. Petersson, *et al.*, *Gaussian 09, Revision B.01*, Gaussian, Inc., Wallingford, CT, 2010.
27 (*a*) A. D. Becke, *J. Chem. Phys.*, 1993, **98**, 5648–5652; (*b*) A. D. Becke, *J. Chem. Phys.*, 1996, **104**, 1040–1046.
28 C. T. Lee, W. T. Yang and R. G. Parr, *Phys. Rev. B: Condens. Matter Mater. Phys.*, 1988, **37**, 785.
29 (*a*) E. G. Hohenstein, S. T. Chill and C. D. Sherrill, *J. Chem. Theory Comput.*, 2008, **4**, 1996–2000; (*b*) V. S. Bryantsev, M. S. Diallo, A. C. T. Duin and W. A. Goddard III, *J. Chem. Theory Comput.*, 2009, **5**, 1016–1026.
30 S. Miertuš, E. Scrocco and J. Tomasi, *J. Chem. Phys.*, 1981, **55**, 117–129.
31 M. Cossi, V. Barone, R. Cammi and J. Tomasi, *Chem. Phys. Lett.*, 1996, **255**, 327–335.
32 (*a*) N. M. O'Boyle, A. L. Tenderholt and K. M. Langner, *J. Comput. Chem.*, 2008, **29**, 839–845; (*b*) R. Dennington, T. Keith and J. Millam, *GaussView, version 5*, Semichem Inc., Shawnee Mission KS, 2009.
33 F. S. Mancilha, B. A. D. Neto, A. S. Lopes Jr, P. F. Moreira, F. H. Quina, R. S. Gonçalves and J. Dupont, *Eur. J. Org. Chem.*, 2006, **21**, 4924–4933.
34 S. Kato, T. Matsumoto, T. Ishii, T. Thiemann, M. Shigeiwa, H. Gorohmaru, S. Maeda, Y. Yamashita and S. Mataka, *Chem. Commun.*, 2004, 2342–2343.
35 I. K. Moon, J. W. Oh and N. Kim, *J. Photochem. Photobiol., A*, 2008, **194**, 351.
36 G. Saikia and P. K. Iyer, *J. Org. Chem.*, 2010, **75**, 2714.
37 (*a*) S. H. Kim, I. Cho, M. K. Sim, S. Park and S. Y. Park, *J. Mater. Chem.*, 2011, **21**, 9139; (*b*) D. P. Hagberg, T. Marinado, K. M. Karlsson, K. Nonomura, P. Qin, G. Boschloo, T. Brinck, A. Hagfeldt and L. Sun, *J. Org. Chem.*, 2007, **72**, 9550.
38 D. W. Price Jr and J. M. Tour, *Tetrahedron*, 2003, **59**, 3131–3156.
39 D. Sahu, C. Tsai, H. Wei, K. Ho, F. Chang and C. Chu, *J. Mater. Chem.*, 2012, **22**, 7945–7953.
40 (*a*) J. Sung, P. Kim, Y. O. Lee, J. S. Kim and D. Kim, *J. Phys. Chem. Lett.*, 2011, **2**, 818–823; (*b*) U. Subuddhi, S. Haldar, S. Sankararaman and A. K. Mishra, *Photochem. Photobiol. Sci.*, 2006, **5**, 459–466.
41 S. Cai, X. Hu, Z. Zhang, J. Su, X. Li, A. Islam, L. Han and H. Tian, *J. Mater. Chem. A*, 2013, **1**, 4763–4772; S. Cai, G. Tian, X. Li, J. Su and H. Tian, *J. Mater. Chem. A*, 2013, **1**, 11295–11305.
42 V. Rajgopal, A. Mahipal Reddy and V. Jayathirtha Rao, *J. Org. Chem.*, 1995, **60**, 7966–7973.
43 V. Rajgopal, V. Jayathirtha Rao, G. Saroja and A. Samanta, *Chem. Phys. Lett.*, 1997, **270**, 593–598.
44 U. Srinivas, P. A. Kumar, K. Srinivas, K. Bhanuprakash and V. Jayathirtha Rao, *J. Struct. Chem.*, 2012, **53**, 851–865.
45 (*a*) A. Baheti, P. Tyagi, K. R. J. Thomas, Y. C. Hsu and J. T. Lin, *J. Phys. Chem. C*, 2009, **113**, 8541–8547; (*b*) Y. J. Chang and T. J. Chow, *Tetrahedron*, 2009, **65**, 4726–4734.
46 C. C. Wu, T. L. Liu, W. Y. Hung, Y. T. Lin, K. T. Wong, R. T. Chen, Y. M. Chen and Y. Y. Chien, *J. Am. Chem. Soc.*, 2003, **125**, 3710–3711.
47 J. Cheng, C. Lin, P. T. Chou, A. Chaskar and K. T. Wong, *Tetrahedron*, 2011, **67**, 734–739.
48 J. Wang, Q. Xiao and J. Pei, *Org. Lett.*, 2010, **12**, 4164–4167.
49 (*a*) K. D. Belfield, S. Yao and M. V. Bondar, *Adv. Polym. Sci.*, 2008, **213**, 97–156; (*b*) J. R. Lakowicz, *Principles of fluorescence spectroscopy*, Springer, 3rd edn, 2006.
50 (*a*) K. R. J. Thomas, J. T. Lin, M. Velusamy, Y. T. Tao and C. H. Chuen, *Adv. Funct. Mater.*, 2004, **14**, 83–90; (*b*) G. Qian, B. Dai, M. Luo, D. Yu, J. Zhan, Z. Zhang, D. Ma and Z. Y. Wang, *Chem. Mater.*, 2008, **20**, 6208–6216.
51 P. Singh, A. Baheti, K. R. J. Thomas, C. P. Lee and K. C. Ho, *Dyes Pigm.*, 2012, **95**, 523–533.
52 (*a*) D. Jacquemin, E. A. Perpéte, G. E. Scuseria, I. Ciofini and C. Adamo, *J. Chem. Theory Comput.*, 2008, **4**, 123–135; (*b*) E. G. Hohenstein, S. T. Chill and C. D. Sherrill, *J. Chem. Theory Comput.*, 2008, **4**, 1996–2000.
53 V. S. Bryantsev, M. S. Diallo, A. C. T. van Duin and W. A. Goddard III, *J. Chem. Theory Comput.*, 2009, **5**, 1016–1026.
54 (*a*) R. E. Martin and F. Diederich, *Angew. Chem., Int. ed.*, 1999, **38**, 1350–1377; (*b*) J. Xia, M. Zhou, S. Sun, G. Wang, P. Song and M. Ge, *Dyes Pigm.*, 2014, **103**, 71–75.
55 M. Ananth Reddy, A. Thomas, K. Srinivas, V. Jayathirtha Rao, K. Bhanuprakash, B. Sridhar, A. Kumar, M. N. Kamalasanan and R. Srivastava, *J. Mater. Chem.*, 2009, **19**, 6172–6184.
56 (*a*) B. M. Wong and J. G. Cordaro, *J. Phys. Chem. C*, 2011, **115**, 18333–18341; (*b*) B. G. Janesko, *J. Chem. Phys.*, 2011, **134**, 184105.
57 D. M. De Leeuw, M. M. J. Simenon, A. R. Brown and R. E. F. Einerhand, *Synth. Met.*, 1997, **87**, 53–59; H. Wang, J. Gao, L. Gu, J. Wan, W. Wei and F. Liu, *J. Mater. Chem. A*, 2013, **1**, 5875–5885.
58 B. Walker, C. Kim and T.-Q. Nguyen, *Chem. Mater.*, 2011, **23**, 470–482.